Structures 64 (2024) 106532

Contents lists available at ScienceDirect

Structures

journal homepage: www.elsevier.com/locate/structures

Developing predictive models for the load-displacement response of laterally loaded reinforced concrete piles in stiff unsaturated clay using machine learning algorithms

K.T. Braun [a,*], G. Markou [a,b], S.W. Jacobsz [a], D. Calitz [c]

[a] Civil Engineering Department Hatfield Campus, University of Pretoria, South Africa
[b] Department of Civil Engineering, Neapolis University Pafos, 2 Danais Avenue, Pafos 8042, Cyprus
[c] SRK Consulting, 265 Oxford Rd, Illovo, Johannesburg, South Africa

ARTICLE INFO

Keywords:
Soil-structure interaction
Machine learning algorithms
Predictive models
Reinforced concrete pile
Horizontal load-displacement response

ABSTRACT

The design of pile foundations that are expected to develop significant lateral loading is a complex procedure that requires the development of objective and accurate design formulae that will not be based on semi-empirical know-how. For this reason, the main objective of this research work is to develop predictive models that will be able to compute the overall mechanical response of reinforced concrete (RC) piles embedded in unsaturated clay. To achieve this goal, experimental data, and advanced nonlinear 3D detailed finite element (FE) modelling were used to construct datasets comprising multiple results related to the ultimate capacity and corresponding horizontal deformation of RC piles that are loaded horizontally until failure. In total, three datasets were developed and then used to train and test predictive models through the use of various machine learning (ML) algorithms. After successfully developing various predictive models, an out-of-sample dataset was developed and used to further validate the accuracy and extendibility of the predictive models. Finally, the most accurate ML-generated predictive model was used to predict the mechanical response of a RC pile embedded in unsaturated clay that was experimentally tested. The ability of the proposed predictive model is demonstrated through this pilot research work.

1. Introduction

When engineers design the foundation systems of any type of structure, design codes that are based on semi-empirical formulae are used. In cases where the design of the foundation involves reinforced concrete (RC) piles that support structures that are expected to develop significant horizontal loads, the current design procedures do not offer the required accuracy. This is due to the lack of accurate design formulae developed based on the real mechanical response of RC piles. For this reason, the development of improved and more accurate design formulae that will be able to predict the capacity of RC piles embedded in soil is of significant importance.

Piled foundations are frequently used as a common type of deep foundation for providing support to structures situated in loose or soft soils. In contrast, shallow foundations are recognized for their incapacity to prevent substantial settlements and shear failure in such soil conditions [36]. Piles can effectively resist vertical loads, lateral loads, or a combination of both. Analysing piles under combined loading is a complex task, as highlighted by Karthigeyan et al. [18], therefore, it is recommended to model the load cases independently [5,33].

It is well known that prior to the development of advanced 3D finite element (FE) models, the soil-structure interaction (SSI) phenomenon proved to be somewhat difficult to define and analyze, as highlighted by Kausel (2010). This difficulty arose from the complex dynamic interactions resulting from the amplification of seismic waves within soil layers, where the nonlinear modelling of RC piles was also challenging, especially when nonlinearities due to large deformations occur ([33]; Braun et al., 2023). Another study conducted by Kavitha et al. [20] examined the nonlinear behaviour of laterally loaded piles, specifically investigating the impact of pile-soil interaction when loaded laterally. The findings indicated that the pile-soil interaction effect was dependent on several factors such as soil properties, loading conditions, ground

* Corresponding author.
E-mail addresses: u17031215@tuks.co.za (K.T. Braun), george.markou@up.ac.za, g.markou@nup.ac.cy (G. Markou), sw.jacobsz@up.ac.za (S.W. Jacobsz), DCalitz@srk.co.za (D. Calitz).

https://doi.org/10.1016/j.istruc.2024.106532
Received 18 February 2024; Received in revised form 14 April 2024; Accepted 2 May 2024
Available online 17 May 2024

slope, as well as the pile material, and diameter.

SSI is a multidisciplinary field encompassing soil mechanics, structural mechanics, and dynamic mechanics, with a focus on understanding the mechanics and interactions between a structure and the soil it is embedded in Kausel [19]. In foundation engineering, SSI analyses predict deformation and stresses in soil interacting with the load structure, crucial for addressing challenges in scenarios such as lateral loads on piles [2,35]. A crucial consideration in the lateral load analysis of piles is the interconnection between the pile deflection and the lateral resistance of the soil domain, referred to as the pile-soil interaction effect [20].

Efforts to capture the elastoplastic behaviour of soil in SSI problems involve solutions with more complex soil property descriptions [17]. The accuracy of predictions is related to determining in-situ elastic moduli parameters and their depth-dependent variations [17]. However, these parameters have proven to be challenging to measure, often producing lower values in conventional laboratory tests compared to field measurements. Field measurements using linear elastic theory for back analysis have seen success, but are limited by occurrences of localized regions displaying fully plastic behaviour, deviating significantly from elastic behaviour [17]. Consequently, obtaining high-quality stress-strain data from SSI problems proves challenging, necessitating sensitivity studies using advanced soil models to explore nonlinearity at small strains and local failures. Despite the evident nonlinear behaviour of soil, current SSI analyses often rely on linear elasticity theories, emphasizing the need for more sophisticated and computationally efficient numerical models.

When analysing the behaviour of piles under lateral loading conditions, Moussa and Christou [30] grouped investigation methods into the following categories:

I. Ultimate Limit State Methods
II. Subgrade Reaction Approaches
III. Continuum Methods
IV. Finite Element Methods

Among these methods, the finite element method (FEM) stands out as the most versatile, prominent, and effective technique, capable of addressing complex problems by accounting for geometrical and material nonlinearities [30]. In recent years, FEM has been extensively used for various structural engineering applications such as analysing the behaviour of RC structures considering damage effects [29], determining the shear capacity of RC deep beams [1], predicting the fundamental period of RC and steel structures [15,40], investigating wind turbine structures [14], and analysing the behaviour of pile foundations [7,33].

The exponential growth of numerical methods has provided realistic and satisfactory results for soil-structure problems, overcoming the limitations associated with traditional approaches [10]. For this reason, the FEM-based software Reconan FEA [34] is used for the needs of this research work. Reconan FEA [34] was also used by Gravett and Markou [14] to conduct a study involving the modelling of battered RC piles embedded in unsaturated clay. Their findings indicated that the efficiency of the Reconan FEA [34] software for accurately capturing the mechanical response of SSI problems was adequate. Building upon the work of Gravett and Markou [14] and incorporating the recent advancements by Braun et al. [7], the current study adopted a similar modelling approach as it will be presented herein.

Even though FEM has allowed the solution of numerous complex problems, the required time for developing 3D detailed models in combination with the specialized know-how that engineers typically do not have, makes its use prohibitive and time-consuming.

Over the past few decades, significant growth and development has been witnessed in the application of Artificial Intelligence (AI) and Machine Learning (ML) in engineering problems, particularly in the domain of structural analysis and design problems [26]. This progress is notable for its effectiveness in handling complex nonlinear structural systems, especially when faced with extreme actions [37]. Furthermore, the integration of AI and ML with validated FE modelling [23] has provided engineers with the capability to evaluate a wide range of engineering applications without the need for physical specimens.

Implementing ML in solving these types of engineering problems [26] involves several key steps, beginning with database preparation, followed by the application of learning algorithms, and concluding with model evaluation. Initial data consists of features (input variables) and target labels (output variables), divided into training and testing sets for effectiveness assessment. During the learning phase, ML algorithms are used to develop predictive models, where various algorithms are compared to identify the most suitable one. Model evaluation and validation are then carried out by assessing overall effectiveness and performance using a separate testing dataset, utilizing error metrics.

Van der Westhuizen et al. [39] have emphasized that ML algorithms do not offer a “one-size-fits-all solution”, and it is crucial to consider different methods to find the most accurate predictive model for a given problem. The primary challenge in ML lies in ensuring good performance on out-of-sample data, a concept known as generalization and extendibility. Furthermore, two critical factors influencing the ML algorithm performance are minimizing the training error and reducing the gap between training and test errors, addressing challenges related to under- and over-fitting [6].

Recently, under the umbrella of the WindAfrica project, researchers conducted an on-site experiment [13] involving RC piles embedded in an unsaturated clay profile. Despite the valuable insights offered by these in-situ experiments, their limitations arise from cost and time constraints, particularly when conducting a parametric investigation involving variations in soil material properties, pile size, and pile material properties. Through advanced 3D detailed numerical modelling, Braun et al. [7] successfully replicated the nonlinear mechanical response of the laterally loaded system, offering insights beyond the experiment’s scope. Braun et al. [7] concluded that their model provided an accurate representation of the experimental response, which was verified through the experimentally obtained horizontal load-displacement curve. Additionally, it was found that Reconan FEA [34] effectively modelled the ultimate failure mechanism, allowing the back-calculation of the actual soil properties that influenced the overall mechanical response of the pile-soil system. This served as the foundation for this research, which aimed to develop various SSI models with RC piles embedded in unsaturated clay to generate numerical results for the construction of a dataset that will consist of ultimate load capacities and their respective horizontal displacements. The generated dataset served as training data for different ML algorithms, allowing the creation of predictive models capable of estimating forces and displacement outputs for various RC pile geometries and soil domains. To validate the predictive models’ capabilities, an additional out-of-sample dataset was developed and used to assess their predictive capabilities on data that were excluded from the training and testing phase. To further validate the proposed predictive models’ accuracy, a comparison was performed through the use of the experimental results presented in Braun et al. [7] and with the proposed predictive models developed and presented in this research work.

2. Material models used for the dataset development

For the purpose of this research work, it is important to investigate the various material models for concrete, steel, and soil. This investigation is based on the incorporation of the models that were outlined in the preparatory work published by Braun et al. [7]. The significance of these models lies in their ability to accurately depict the mechanical response of the pile-soil system, and accordingly, they have been integrated into the Reconan FEA [34] software.

The Kotsovos and Pavlovic [21] concrete material model, as modified by Markou and Papadrakakis [24], was used to model the concrete

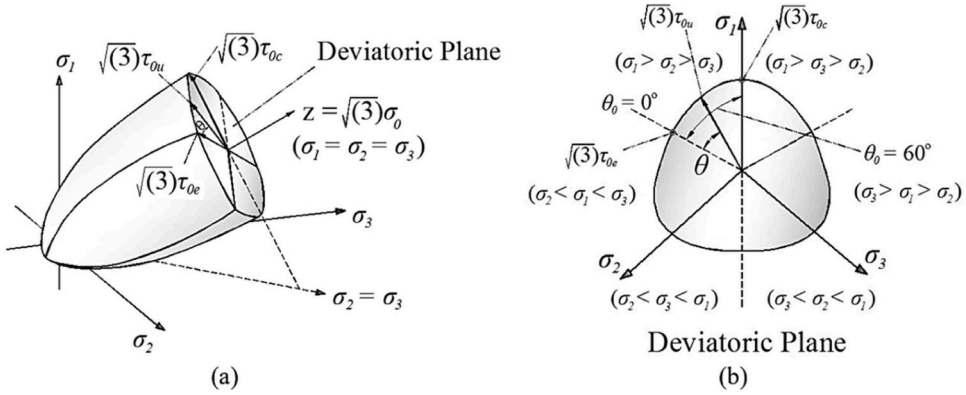

Fig. 1. Continuous plastic strain of an elastic-perfectly plastic material [24].

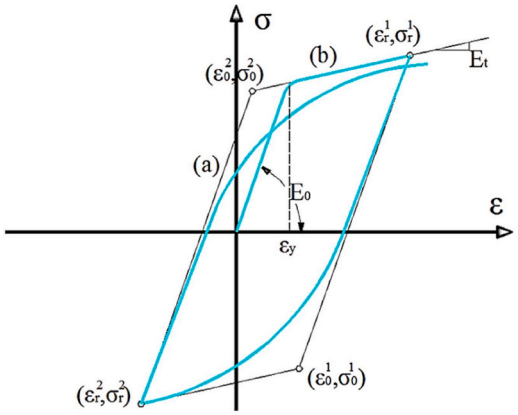

Fig. 2. Continuous plastic strain of an elastic-perfectly plastic material [22].

material for the needs of this study. This material model was created through a process of numerical regression using experimental data from concrete specimens subjected to both uniaxial and triaxial stress conditions [25]. The consideration of out-of-plane stresses is a fundamental aspect of 3D modelling. According to this concrete material model, the stress-strain relationship for each stress state is described by two components: the hydrostatic (σ_0) and deviatoric (τ_0) components. Gravett and Markou [14] recently presented a study that explains how the corresponding hydrostatic and deviatoric strains (ε_0, γ_0) are utilized to calculate the hydrostatic and deviatoric stresses when used for different FE sizes. The Willam [42] formula (Eq. 1) presents the formulation that describes the strength envelope of concrete [21]. When the failure surface is projected onto the deviatoric plane perpendicular to σ_0, it forms a convex curve (Fig. 1) that represents the geometric path of the ultimate deviatoric stress.

$$\tau_{0u} = \frac{2\tau_{0c}\left(\tau_{0c}^2 - \tau_{0e}^2\right)\cos\theta + \tau_{0c}(2\tau_{0e} - \tau_{0c}) \times SQ}{4(\tau_{0c}^2 - \tau_{0e}^2)\cos^2\theta + (2\tau_{0e} - \tau_{0c})^2} \tag{1}$$

Where:

$$SQ = \sqrt{4\left(\tau_{0c}^2 - \tau_{0e}^2\right)\cos^2\theta + 5\tau_{0e}^2 - 4\tau_{0c}^2\tau_{0e}^2}$$

In Eq. 1, θ denotes the angle of rotation between the deviatoric stress vector and one of the principal stress axes projected on the deviatoric plane. Fig. 1 also highlights τ_{0e} and τ_{0c} as the deviatoric stresses that develop at angles of $\theta = 0^\circ$ and $\theta = 60^\circ$, respectively. In addition, upon meeting the failure criteria, the model adopts a smeared crack approach in which macro-cracking is simulated [24]. The model presented in this section is also the method adopted for the needs of this research work.

The available constitutive material models for predicting the steel behaviour of reinforcement include the nonlinear Menegotto and Pinto material model (Fig. 2), which has been enhanced with the isotropic strain hardening by Filippou et al. [12], as well as the standard bilinear steel material model. The Reconan FEA [34] software incorporates the Menegotto-Pinto method, which accounts for the Bauschinger effect to ensure comprehensive analysis and accurate results [27]. The Menegotto and Pinto material model is widely acknowledged for its straightforward numerical formulation, which offers the essential tools to predict the behaviour of steel elements, such as rebars, with a satisfactory level of accuracy [22]. The stress-strain relationship for the steel material is represented in Eq. 2.

$$\sigma^* = b\varepsilon^* + \frac{(1-b)\varepsilon^*}{\left(1+\varepsilon^{*R}\right)^{1/R}} \tag{2}$$

Where the strain hardening ratio is denoted as b. The normalized stress and strain are expressed in Eqs. 3 and 4, respectively.

$$\sigma^* = \frac{(\sigma - \sigma_r)}{(\sigma_0 - \sigma_r)} \tag{3}$$

$$\varepsilon^* = \frac{(\varepsilon - \varepsilon_r)}{(\varepsilon_0 - \varepsilon_r)} \tag{4}$$

Additionally, the parameter R (Eq. 5) influences the shape of the transition curve and enables an accurate representation of the Bauschinger effect [11].

$$R = R_0 - \frac{a_1\xi}{(a_2 + \xi)} \tag{5}$$

Where the parameter ξ represents the normalized plastic strain, R_0 denotes the value of R during the initial yielding loading, while the parameters a_1 and a_2 are experimentally derived to describe the decrease in curvature with each subsequent cycle.

When it comes to soil modelling, the incorporation of elasticity, plasticity, and friction offers several possibilities for representing soil behaviour. Over the past three decades, several researchers have tried to understand and predict the nonlinear behaviour of different soil aspects by developing various constitutive models. These models are also utilized in FE modelling for applications in geotechnical engineering. However, the behaviour of soils in practice is highly complex, exhibiting a wide range of responses under different loading conditions [38]. As discussed by Ti et al. [38], there is currently no soil constitutive model that can fully describe the complex behaviour of real soils when considering all conditions.

Atkinson and Bransby [3] identified three distinct behaviours in the stress-strain relationship: elastic-perfectly plastic, elastic-plastic hardening, and elastic-plastic softening. For the purpose of this research work, the soil material was modelled to behave in a simple elastic-perfectly plastic manner, using a von Mises yielding criterion. In

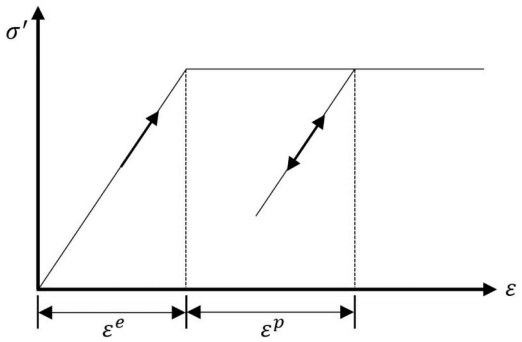

Fig. 3. Continuous plastic strain of an elastic-perfectly plastic material (as adapted from Park [31]).

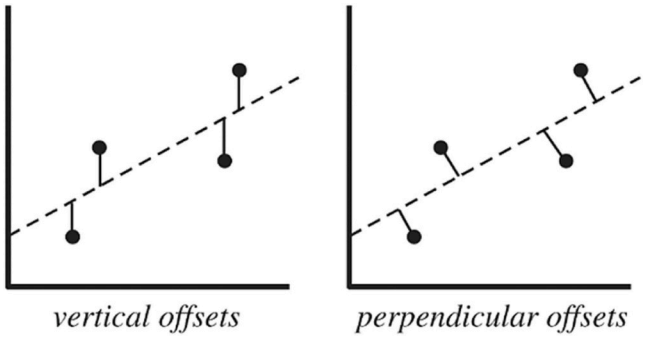

Fig. 4. Vertical and perpendicular offset for least squares fitting [41].

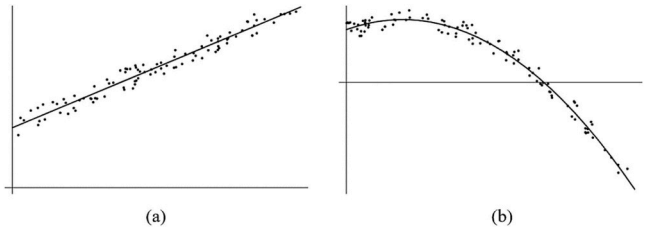

Fig. 5. Least squares fitting showing the best-fit line (a) and best-fit polynomial (b) [41].

this behaviour (Fig. 3), constant stress leads to continuous strain, resulting in plastic deformation occurring under plastic strain (ε^p). The material undergoes elastic strain (ε^e) before experiencing plastic strain, and beyond the yield point, continued deformation occurs without changes in stress. This perfectly plastic behaviour during plastic deformation allows the soil to retain the same stress state without any increase in stress during unloading [3].

3. Machine learning algorithms

In this section, all the ML algorithms used to meet the objectives of this study are presented. A variety of ML algorithms proposed by Markou et al. [26] was used, including polynomial regression with hyperparameter tuning (POLYREG-HYT), extreme gradient boosting with hyperparameter tuning, and cross-validation (XGBoost-HYT-CV), random forests with hyperparameter tuning (RF-HYT), artificial neural networks by neighbourhoods (ANNbN), and deep learning with hyperparameter tuning with a message-passing interface (MPI) and Horovod (DANN-MPIH-HYT). The linear regression (LR), which was also used as the base algorithm in this work, and the POLYREG-HYT algorithm have the advantage of deriving an explicit closed-form formula, whereas XGBoost-HYT-CV, RF-HYT, ANNbN, and DANN-MPIH-HYT generate a "black-box" solution.

In the case of the LR ML algorithm, it utilizes the least squares fitting approach to determine the optimal curve fitting through a given set of points. This involves minimizing the sum of squared residuals, which are vertical and perpendicular offsets between points and the curve, as illustrated in Fig. 4. The squared approach may be impacted by extreme outliers. Residuals, representing differences between observed and predicted outcomes, help assess the fit's quality. Eq. 6 expresses the vertical least squares fitting technique for a collection of n datapoints, which is a foundational LR method. Fig. 5 shows its extension to polynomials, where the residuals for k^{th}-degree polynomials are defined in Eq. 7.

$$R^2 = \sum [y_i - f(x_i, a_1, a_2, \ldots, a_n)]^2 \tag{6}$$

$$R^2 = \sum_{i=1}^{n} \left[y_i - \left(a_0 + a_1 x_i + \ldots + a_k x_i^k\right)\right]^2 \tag{7}$$

Polynomial regression (PR) involves least squares to fit a curve (Fig. 5b), linking dependent and independent variables. LR serves as the basis for simple relationships, while multiple linear regression extends LR to incorporate multiple predictors. PR provides flexibility to fit nonlinear data, with polynomial degree determining model complexity. This research adopts a PR ML algorithm with hyperparameter tuning, POLYREG-HYT, that identifies nonlinear features, enhancing prediction accuracy. The POLYREG-HYT algorithm [26] automates the derivation of closed-form prediction formulae, offering computational efficiency. This algorithm uses nonlinear combinations of independent variables up to a desired degree. It automatically identifies nonlinear features with the least prediction error, rapidly reducing combinations with increasing features and polynomial degrees. Eq. 8 defines the relationship between combination number (c), number of features (n), and polynomial degree (k). Due to the limited nature of datasets, selecting the most appropriate nonlinear feature is crucial to enhance algorithmic performance. Consequently, the maximum number of features m is constrained to ensure enough degrees-of-freedom (DOFs) for regression and obtaining statistically reliable outcomes (Eq. 9). The study employs an improved feature selection algorithm, an advancement in embedded optimization for polynomial feature selection. The algorithm's objective is to identify indices to minimize regression error during iterations, enhancing feature selection efficiency [26].

$$c = \left(\binom{n}{k}\right) = \binom{n+k-1}{k} = \frac{(n+k-1)!}{k!(n-1)!} \tag{8}$$

$$c_f = \binom{c}{m} = \frac{(c)!}{k!(m-k)!} \tag{9}$$

Extreme gradient boosting (XGBoost) is a powerful gradient-boosting library designed for supervised learning tasks like classification and regression [28]. Known for speed and scalability, it handles large, high-dimensional datasets, addressing challenges such as missing values and imbalanced classes. To address overfitting, XGBoost incorporates built-in features for feature selection and regularization, which is a common concern in the field of ML [26]. XGBoost is based on decision trees (DTs), which, while prone to overfitting, become robust when combined in an ensemble [37]. The study introduces hyperparameters, while also including grid search with cross-validation (XGBoost-HYT-CV) to optimize the training process. The hyperparameters considered include the number of rounds, tree depth, learning rate, and subsample [26]. The inclusion of k-fold cross-validation [32] enhances evaluation robustness, balancing between computational efficiency and accurate hyperparameter tuning.

Random Forests (RF) is a robust ML algorithm developed by Breiman [8], that significantly impacts various scientific fields, offering high accuracy and versatility. This ensemble learning method combines multiple DTs, addressing overfitting by aggregating predictions through

Table 1
Geometrical parameters.

Geometrical Parameter	Value	Units
Pile Diameter (D)	20, 30, 40, 50, 60, 70, 80, 90, 100	cm
Embedded Pile Depth (H)	6, 9, 12	m
Reinforcement Ratio (ρ)	0.5, 2, 4	%

majority voting or averaging [37]. RF is effective in both classification and regression, excelling in handling large datasets. Markou et al. [26] introduced RF-HYT, a hyperparameter tuning approach, focusing on crucial parameters such as the number of DTs, maximum tree depth, partial sampling, subfeatures' percentage, and the minimum samples at a leaf node. These parameters enhance RF's performance and stability, with the flexibility to control model complexity, variance, and robustness. The default parameters in RF are generally effective, but hyperparameter tuning provides a means to optimize for specific tasks, offering a trade-off between accuracy and computational efficiency.

The Artificial Neural Network (ANN), widely used in ML and data mining, emulates the human brain's intricate neural networks, offering advantages in discovering patterns without predefined constraints [16]. The ANN's architecture includes input layers, hidden layers, and output layers, enabling the identification of complex nonlinear relationships in data. The ANNbN ML algorithm [4] utilized in this study, introduces a new approach by dividing responses into clusters (or neurons), calculating weights for each cluster, and aggregating them for a global approximation (global weight v_k and biases b_0). The training process involves computing local weights (w_{jk}) and biases (b_k), crucial for adjusting network parameters [4]. The ANNbN ensemble further enhances performance by averaging outcomes across multiple models, trained on distinct data segments. This ensemble strategy, detailed in Bakas et al. [4], leads to improved generalization and overall performance for the ANNbN ML algorithm.

Lastly, this research focuses on implementing Deep Learning (DL) using ANNs with hyperparameter tuning, specifically employing message-passing interface (MPI) and Horovod. This methodology, referred to as DANN-MPIH-HYT, leverages DL's foundation in neural networks to address complex tasks. The DL process involves replicating the human brain's architecture, where interconnected nodes in hidden layers facilitate the understanding of intricate patterns [9]. However, the deep nature of DL architectures demands significant computational resources, often necessitating parallel training on GPUs. Markou et al. [26] outline the integration of Horovod and MPI in the DANN-MPIH-HYT algorithm, which was used for the needs of this research work.

4. Development of numerical models and dataset

The primary objective of this research work is to establish a large dataset that includes multiple SSI numerical models. The models developed herein were based on the validated numerical model presented by Braun et al. [7]. These numerical models encompass a variety of geometrical configurations, incorporating changes in pile diameter, embedded pile depth, and the reinforcement ratio of RC piles. Additionally, a range of material properties, including Young's moduli and the compressive strength of both concrete and soil, are taken into account. Through the use of the newly developed open-source *Notebook for Machine Learning* (nbml) software,[1] the developed dataset was used as input for the training and testing of ML algorithms.

The research utilized a modelling technique based on the work by Braun et al. [7] to develop numerical models for laterally loaded piles in stiff unsaturated clay. A total of 81 base models were created, varying in geometric configurations (see Table 1) such as pile diameter (D),

[1] https://github.com/nbakas/nbml/blob/main/docs/_nbml_.pdf

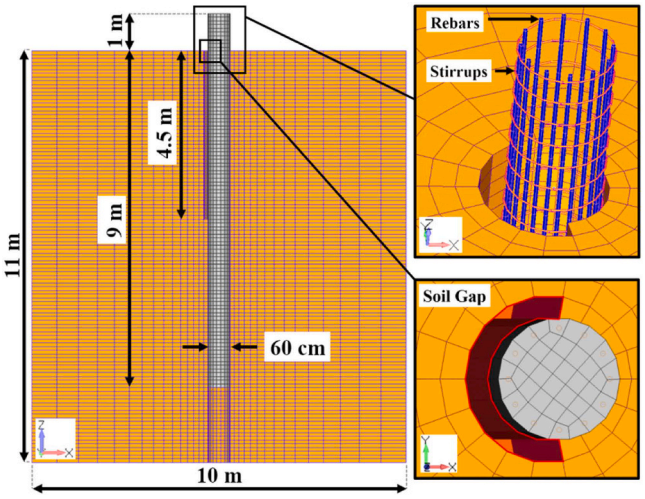

Fig. 6. Base model with a D of 60 cm, H of 9 m, and ρ of 2 %; reinforcement layout and interface of pile and soil detachment.

Table 2
Material parameters that were considered for the development of the numerical models.

Material Parameter	Value	Units
Soil Young's modulus (E_{soil})	50, 100, 150	MPa
Soil compressive strength (CS_{soil})	20, 85, 150	kPa
Concrete Young's modulus (E_{con})	20, 40, 60	GPa
Concrete compressive strength (CS_{con})	20, 40, 60	MPa

embedded pile depth (H), and reinforcement ratio (ρ). The FE Pre- and Post-processing modelling software FEMAP was employed, with auto-discretization using 8-noded isoparametric solid hexahedral FEs for both the concrete piles and surrounding soil. Hexahedral element sizes were adjusted based on the pile diameter to optimize computational efficiency. Tension elements behind the pile were removed up to 0.5H depth, following the "Gap" model proposed by Braun et al. [7]. Similar to that of Braun et al. [7], the reinforcement of the pile was discretized through the use of embedded rod elements. Longitudinal reinforcement diameters were determined considering specified reinforcement ratios, resulting in 12 equally positioned rebars with a concrete cover of 50 mm, while 10 @ 150 stirrups were assumed throughout all pile diameters for all numerical models. Fig. 6 illustrates 1 of the 81 base models, while also providing a detailed view of the pile reinforcement layout and the removal of tension elements behind the pile. The interface between the concrete and unsaturated clay hexahedral elements was assumed to be fully bonded, as described by Braun et al. [7].

The numerical models in this research incorporated both constant and varying material properties as parameter inputs. Constant properties adopted by Braun et al. [7], including soil's Poisson's ratio (0.3), concrete's Poisson's ratio (0.2), concrete's strength under tension (2 MPa), 5 % of remaining concrete shear strength, and an elastic concrete limit of 50 % (Markou and Papadrakakis, 2013), were maintained across all models. Steel properties, such as Young's modulus of 200 GPa, a Poisson's ratio of 0.3, a yield strength of 500 MPa, and a steel strain failure of 12 %, were consistently applied. Varying material properties considered minimum, medium, and maximum values as shown in Table 2, totalling 81 combinations for concrete and soil input features. These material variations, employed in 81 base models with diverse geometries, resulted in 6561 numerical models analyzed through Reconan FEA [34], providing a comprehensive exploration of multiple pile-soil combinations.

As it was reported by Braun et al. [7], their model was calibrated using the WindAfrica project's field experiment, where the horizontal

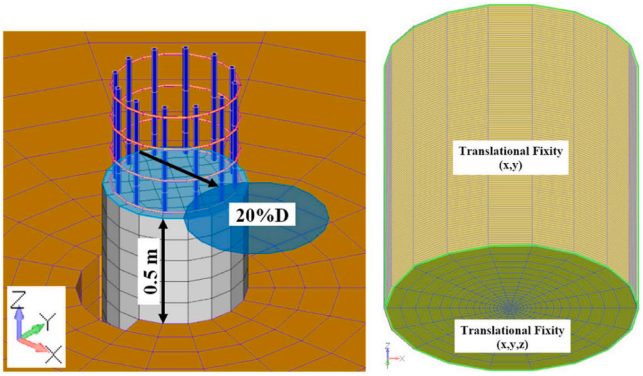

Fig. 7. Location and magnitude of imposed displacement for 60 cm pile diameter (left), and translational fixity (right).

boundaries, and translational restraints along the x, y, and z directions at the domain's bottom, as depicted in Fig. 7 (right).

Using the FEMAP application programming interface, a visual basic analysis (VBA) code (see Appendix A1) was used to replicate each of the 81 base models by considering each possible combination of material property input, reproducing 6561 different numerical models containing all geometrical and material property combinations. The resulting neutral input files (with a total combined size of 41 GB) were then analyzed through Reconan FEA [34] using a Python multi-run code (see Appendix A2), producing 5.7 TB of output files. Post-simulation, a second Python code (see Appendix A3) extracted relevant results from output files, storing data in Excel spreadsheets, including the number of displacement increments, horizontal failure force, horizontal failure displacement, and the horizontal displacement at half the failure force. It is important to note that it was selected to use results from models that achieved at least 10 displacement increments ($NR \geq 10$) during the

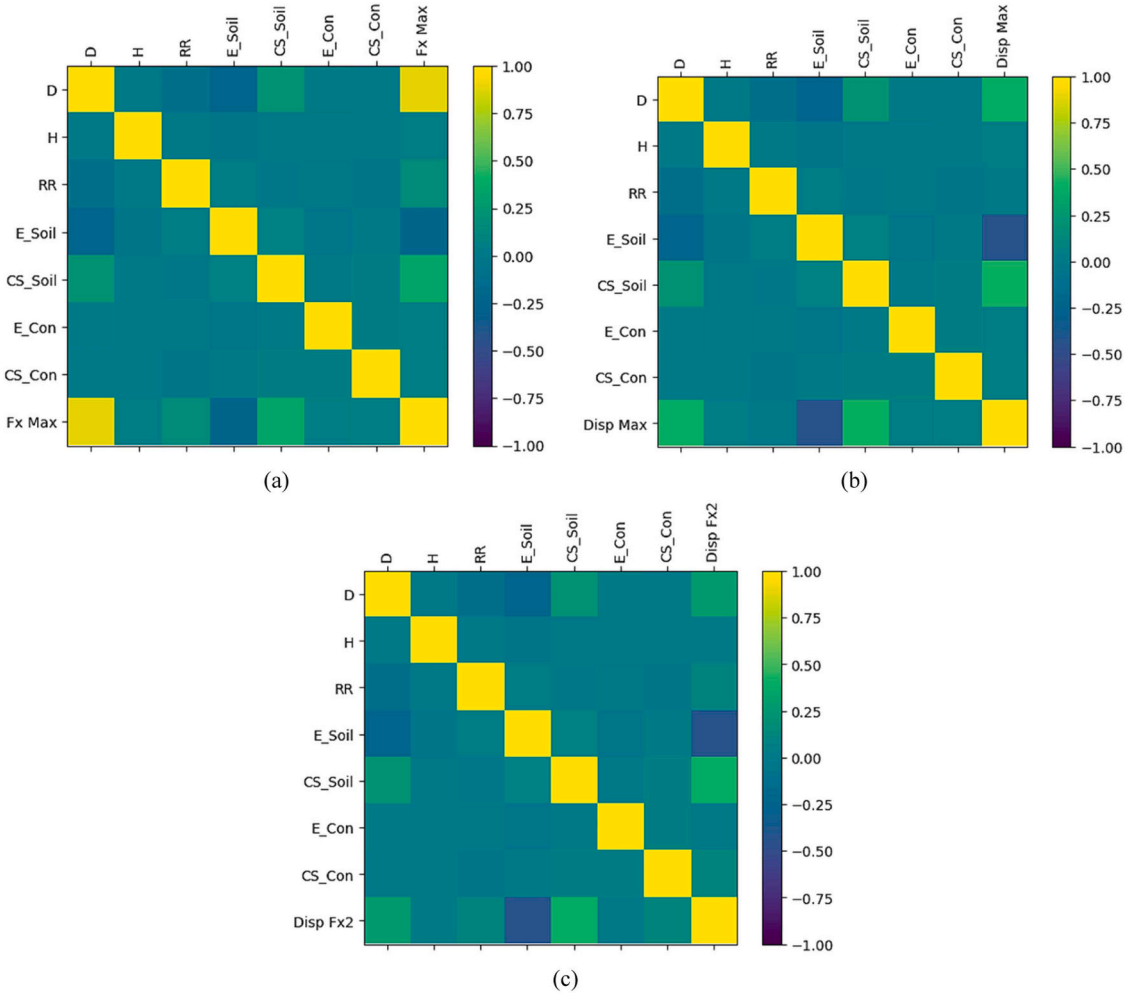

Fig. 8. Correlation matrix for all independent features and target variables with (a) *Fx Max*, (b) *Disp Max*, and (c) *Disp Fx2*.

load was applied to piles at a height of 0.5 m above the soil surface. Therefore, to simulate this experimental setup, it was decided to perform nonlinear static pushover analyses that involved the application of horizontal displacements (x-global axis) equal to 20 % of the pile diameter, as illustrated in Fig. 7 (left). A displacement-controlled Newton-Raphson algorithm incorporated in Reconan FEA [34] was used, where the imposed displacement was applied through the use of 40 displacement increments. The soil cylindrical domain had translational restraints in the x and y directions along the perimeter

nonlinear analysis, deliberately excluding instances of premature failure. By adopting the criterion of $NR \geq 10$, the number of models that were eventually selected for the final dataset was reduced to 2529. This selection ensured a sufficient number of data points, thus preserving the full range of minimum, medium, and maximum geometrical and material property parameters.

As it was described by Markou et al. [26], the structure of the input dataset required by the nbml software necessitates a specific tabular format. This prescribed format requires all of the input features

Table 3
Fx Max performance metrics.

ML Method	Dataset	Pearson (%)	MAPE (%)	MAMPE (%)	MAE	RMSE	alpha	beta
LR	Train	89.14	76.77	30.82	86.041	122.825	0.750	80.249
LR	Test	88.77	80.21	33.49	93.710	136.028	0.705	86.211
POLYREG-HYT-3	Train	98.53	18.97	10.81	30.182	45.812	0.971	7.922
POLYREG-HYT-3	Test	98.48	20.43	11.91	33.313	50.899	0.942	15.689
XGBoost-HYT-CV	Train	99.11	13.24	8.54	23.845	35.709	0.980	5.498
XGBoost-HYT-CV	Test	98.71	14.77	10.41	29.121	47.147	0.946	14.487
RF-HYT	Train	99.10	9.81	7.69	21.472	36.055	0.968	8.967
RF-HYT	Test	98.52	**13.02**	10.56	29.548	52.206	0.916	21.156
ANNbN	Train	98.38	31.88	11.72	32.708	48.090	0.968	8.981
ANNbN	Test	86.12	62.15	34.21	95.731	147.833	0.699	80.016
DANN-MPIH-HYT	Train	92.45	49.57	25.26	70.533	105.994	0.760	64.442
DANN-MPIH-HYT	Test	92.38	53.35	26.88	75.206	118.851	0.720	69.001

Table 4
Disp Max performance metrics.

ML Method	Dataset	Pearson (%)	MAPE (%)	MAMPE (%)	MAE	RMSE	alpha	beta
LR	Train	63.83	25.90	23.23	0.010	0.013	0.477	0.022
LR	Test	66.10	26.48	23.86	0.010	0.013	0.513	0.020
POLYREG-HYT-3	Train	74.00	23.02	19.79	0.008	0.011	0.548	0.019
POLYREG-HYT-3	Test	71.89	24.92	21.42	0.009	0.012	0.551	0.019
XGBoost-HYT-CV	Train	78.40	20.82	17.97	0.008	0.010	0.597	0.017
XGBoost-HYT-CV	Test	72.65	**24.20**	20.59	0.009	0.011	0.570	0.018
RF-HYT	Train	80.73	19.83	17.04	0.007	0.010	0.612	0.017
RF-HYT	Test	71.81	24.69	20.71	0.009	0.012	0.562	0.019
ANNbN	Train	75.77	22.16	19.22	0.008	0.011	0.574	0.018
ANNbN	Test	66.83	27.66	23.74	0.010	0.012	0.509	0.021
DANN-MPIH-HYT	Train	76.12	22.25	19.83	0.008	0.011	0.454	0.021
DANN-MPIH-HYT	Test	72.16	25.09	21.90	0.009	0.012	0.438	0.022

Table 5
Disp Fx2 performance metrics.

ML Method	Dataset	Pearson (%)	MAPE (%)	MAMPE (%)	MAE	RMSE	alpha	beta
LR	Train	59.46	24.67	21.97	0.003	0.003	0.449	0.007
LR	Test	61.11	24.94	22.50	0.003	0.003	0.501	0.006
POLYREG-HYT-3	Train	74.10	20.19	17.55	0.002	0.003	0.549	0.005
POLYREG-HYT-3	Test	70.14	22.07	19.01	0.002	0.003	0.545	0.006
XGBoost-HYT-CV	Train	77.48	18.90	16.41	0.002	0.003	0.577	0.005
XGBoost-HYT-CV	Test	70.41	**21.59**	18.60	0.002	0.003	0.549	0.005
RF-HYT	Train	81.32	17.03	15.00	0.002	0.002	0.600	0.005
RF-HYT	Test	69.72	21.76	18.65	0.002	0.003	0.526	0.006
ANNbN	Train	74.31	19.80	17.39	0.002	0.003	0.552	0.005
ANNbN	Test	58.00	27.03	23.50	0.003	0.003	0.467	0.006
DANN-MPIH-HYT	Train	62.84	25.84	21.35	0.003	0.003	0.269	0.009
DANN-MPIH-HYT	Test	60.65	28.26	22.44	0.003	0.003	0.260	0.009

occupying the first set of columns, followed by the target variable positioned in the last column, with each column denoted by its respective parameter name. Therefore, the complete dataset underwent further refinement into three distinct datasets for target variables:

i. maximum horizontal failure force (*Fx Max*),
ii. horizontal displacement at failure force (*Disp Max*), and
iii. horizontal displacement at half failure force (*Disp Fx*2).

These three datasets, which are available online,[2] were then used to develop the predictive models that are proposed in this manuscript for the prediction of the capacity and horizontal deformation of RC piles embedded in unsaturated clay.

5. Proposed predictive machine learning models

In this section, the results of the LR-generated model as well as the proposed predictive models obtained from the five enhanced ML algorithms (POLYREG-HYT, XGBoost-HYT-CV, RF-HYT, ANNbN, and DANN-MPIH-HYT), will be presented, analyzed, and discussed. In order to develop a predictive model, the three distinct datasets served as input into ML algorithms within the nbml software, which was then trained and tested using an 85–15 train-test ratio. According to the developed datasets, the following seven input features with their specified units were assumed:

D	pile diameter (cm)
H	embedded pile depth (m)
RR	reinforcement ratio ρ of the longitudinal reinforcement in the pile (%)
E_{soil}	Young's modulus of the clay soil material (MPa)
CS_{soil}	Uniaxial compressive strength of the clay soil material (kPa)
E_{con}	Young's modulus of the concrete pile (GPa)
CS_{con}	concrete's compressive strength of the pile (MPa)

[2] https://github.com/nbakas/nbml/

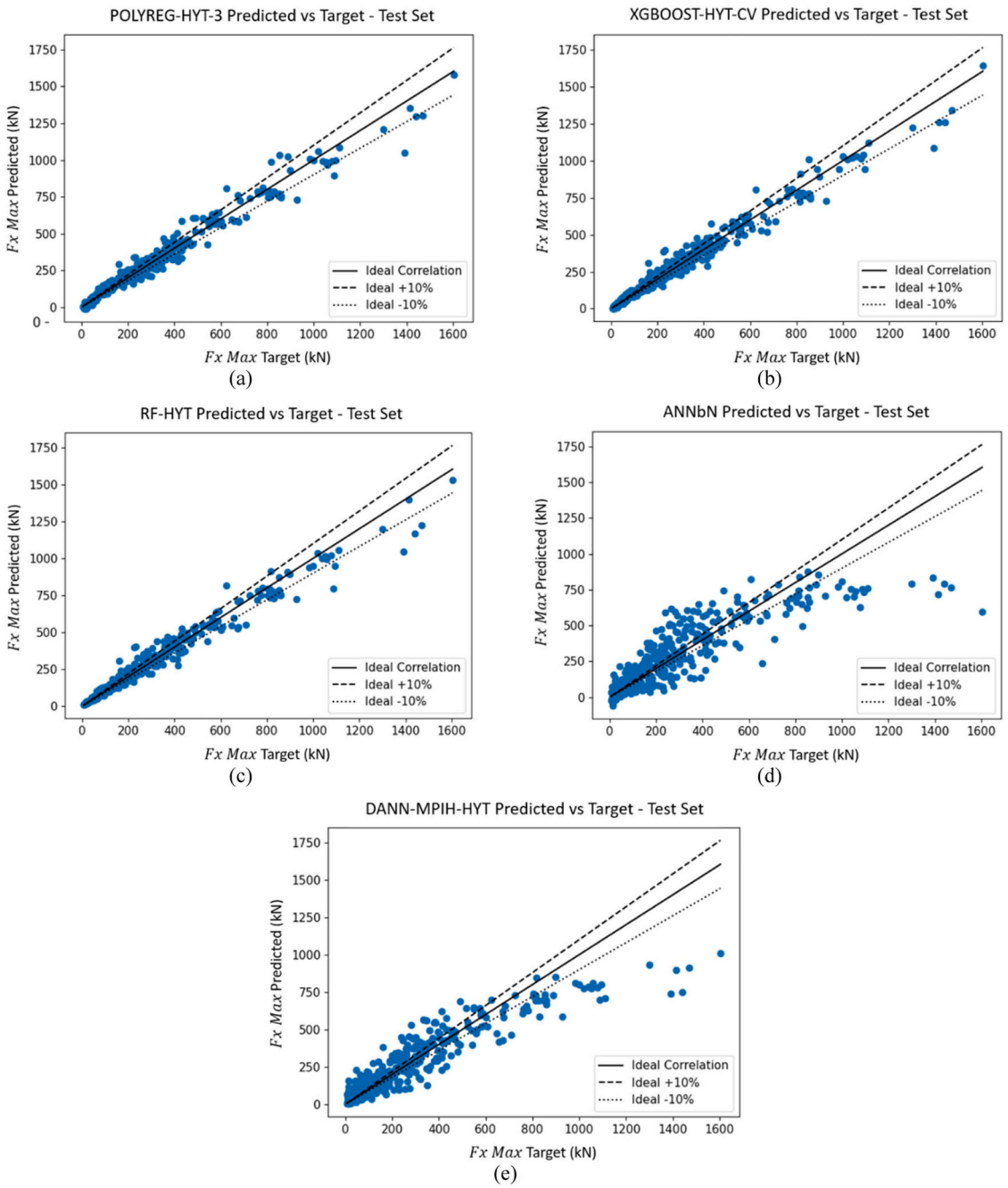

Fig. 9. Test set target versus predicted plot for *Fx Max*. (a) POLYREG-HYT-3, (b) XGBoost-HYT-CV, (c) RF-HYT, (d) ANNbN, (e) DANN-MPIH-HYT.

Before presenting the prediction accuracy of the various ML-generated models, a descriptive analysis was performed for each of the 3 developed datasets. Fig. 8 presents the correlation matrix for all of the seven input features, along with the correlations of the three different target values. It is easy to observe that the correlations of E_{soil} and CS_{soil} with D are stronger compared to the rest. When observing the correlation between *Fx Max* (pile's ultimate horizontal load capacity) and the input features (Fig. 8a), a strong positive correlation is evident between D and *Fx Max*. Additionally, E_{soil} and CS_{soil} exhibit reasonably strong correlations with D and *Fx Max*, which is a finding that aligns with the findings during the parametric investigation presented by Braun et al. [7]. Fig. 8(b) and (c) yield similar results in terms of the correlation between *Disp Max* (maximum horizontal displacement at ultimate load capacity) and *Disp Fx*2 (horizontal displacement at half of the ultimate load capacity).

After employing the six ML methods, the performance metrics for predicting the three target variables (*Fx Max*, *Disp Max*, and *Disp Fx*2) are presented in Tables 3, 4, and 5, respectively. These tables provide insights into the model performance during both training and testing phases, with metrics such as Pearson correlation, Mean Absolute Percentage Error (MAPE), Mean Absolute Mean Percentage Error (MAMPE), Mean Absolute Error (MAE), Root Mean Squared Error (RMSE), alpha, and beta. Figs. 9, 10, and 11 present the Target versus Predicted plots for each target variable in the test set, offering performance plots of the five enhanced ML models.

For the *Fx Max* target variable (Table 3), the RF-HYT method exhibits the best performance on the test set (Fig. 9c), achieving the lowest MAPE of 13.02 %. This method also demonstrates high Pearson correlation (98.52 %) and low errors across other metrics, indicating its accuracy in predicting the horizontal failure force. The XGBoost-HYT-CV

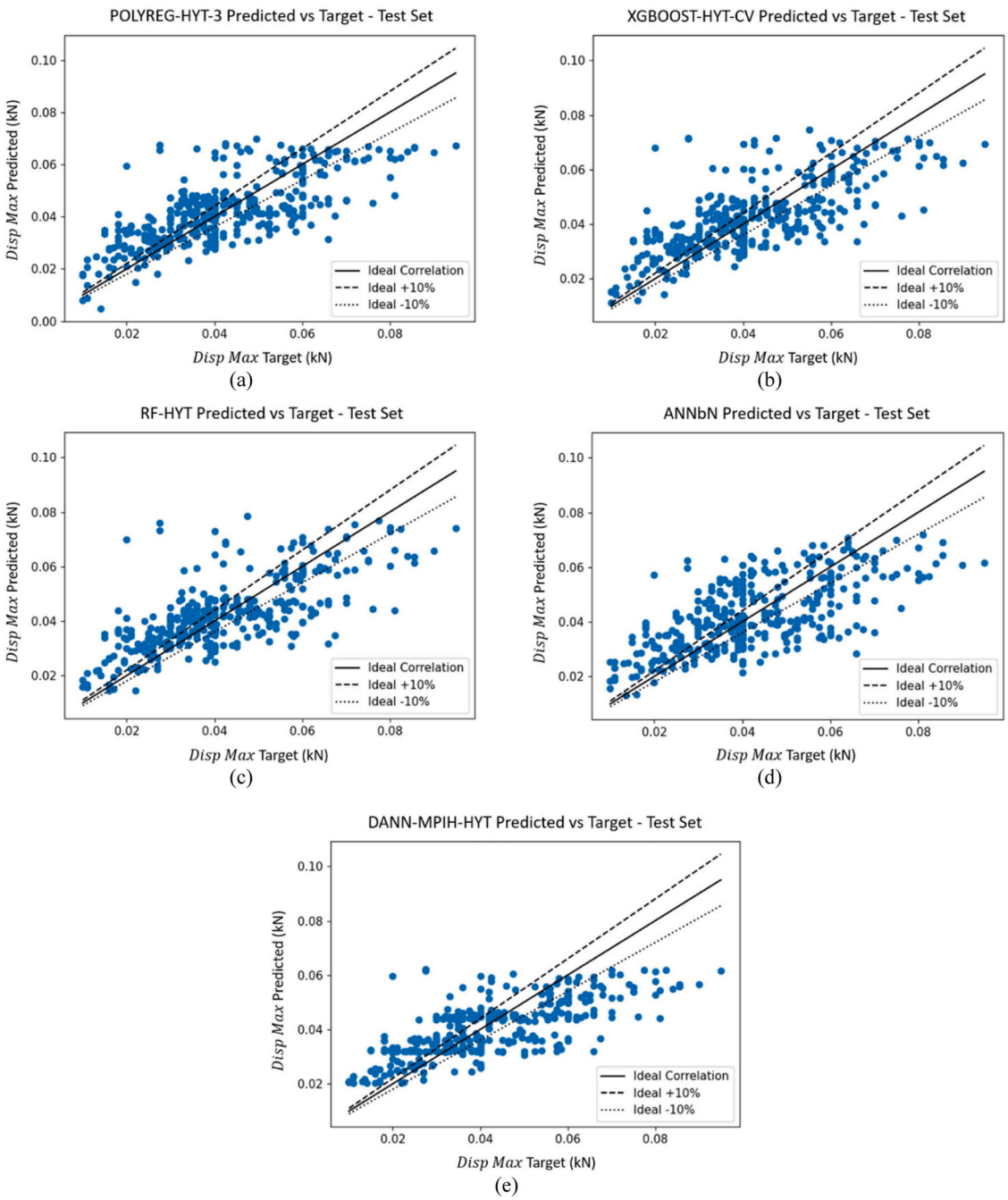

Fig. 10. Test set target versus predicted plot for *Disp Max*. (a) POLYREG-HYT-3, (b) XGBoost-HYT-CV, (c) RF-HYT, (d) ANNbN, (e) DANN-MPIH-HYT.

method performs second best in terms of MAPE on the test set, achieving a value of 14.77 %, while obtaining the highest Person correlation (98.71 %) among all other methods for the test set (Fig. 9b). The POLYREG-HYT-3 method also performs well, with a MAPE of 20.43 % and a slight reduction in Pearson correlation, obtaining a value of 98.48 % on the test set (Fig. 9a).

In the case of *Disp Max* (see Table 4), the XGBoost-HYT-CV method outperformed all methods when used on the test set (Fig. 10b), achieving the lowest MAPE (24.20 %). XGBoost-HYT-CV is closely followed by the RF-HYT method (Fig. 10c) and then by the POLYREG-HYT-3 method (Fig. 10a), which achieved a MAPE of 24.69 % and 24.92 %, respectively. It is important to note here that the POLYREG-HYT-3 method assumes a 3rd-degree polynomial order, generating closed-form formulae for each target variable (see Appendix A4.1, A4.2, and A4.3, respectively). According to the numerical analysis, these three methods demonstrated relatively weak Pearson correlations (72.65 %, 71.81 %, and 71.89 % for the test set, respectively) and low errors in MAE and RMSE. This is attributed to the double nonlinearities that control the horizontal deformation of the RC piles near the failure load. Concrete cracking, rebar yielding, and soil plastification are the major mechanical phenomena that determine the final deformed shape, rendering this SSI problem highly nonlinear and in many cases unpredictable.

For the case of predicting the *Disp Fx*2 (see Table 5), the XGBoost-HYT-CV method again emerges as the top performer for the test set (Fig. 11b), with a MAPE being equal to 21.59 %. The RF-HYT method (Fig. 11c) follows with a MAPE of 21.76 %, and then the POLYREG-HYT-3 method (Fig. 11a) with a MAPE of 22.07 %. These methods showcase slightly weaker Pearson correlations than that of *Disp Max* (70.41 %, 69.72 %, and 70.14 % for the test set, respectively) and exhibit low errors in terms of MAE and RMSE.

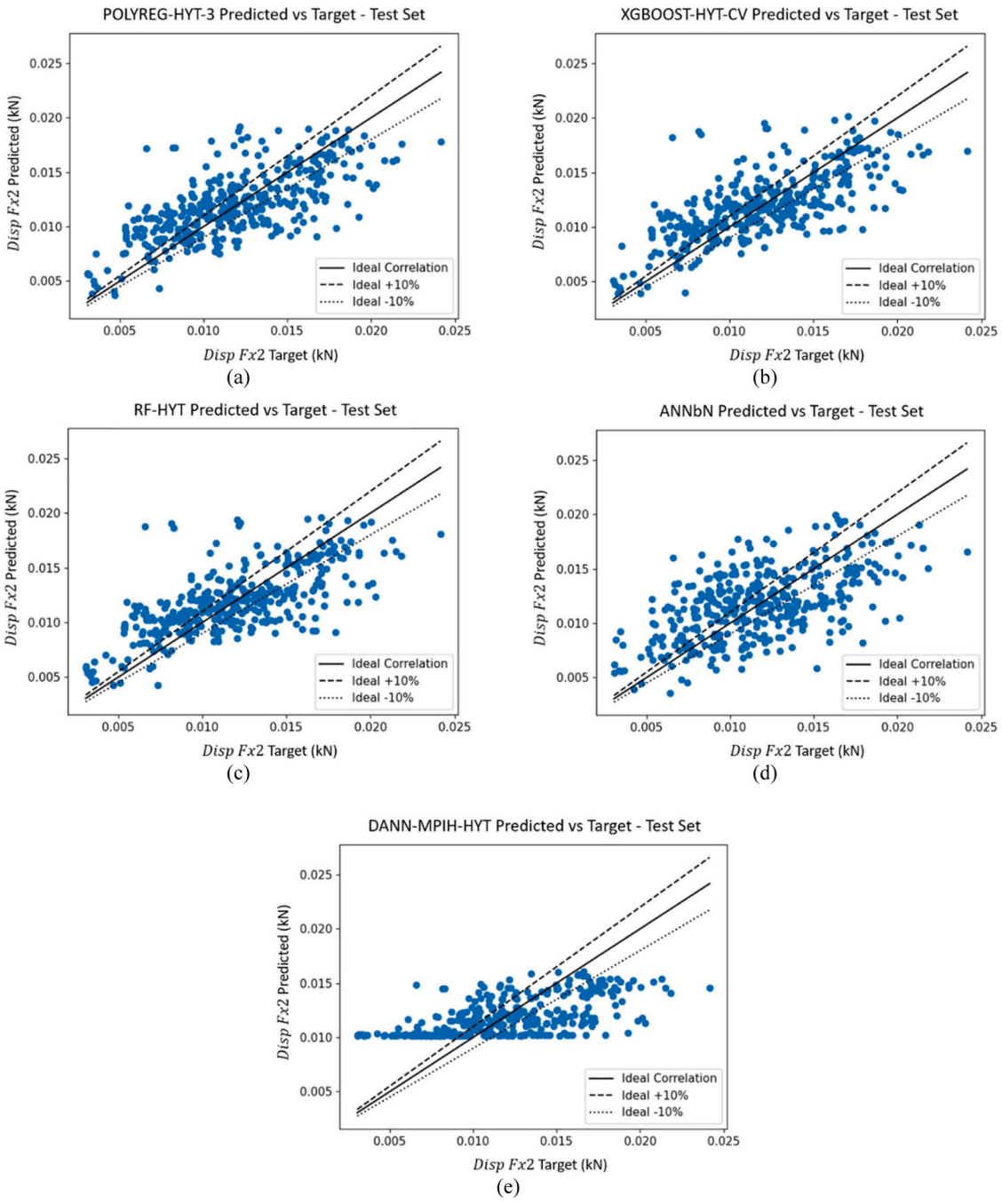

Fig. 11. Test set target versus predicted plot for *Disp Max*. (a) POLYREG-HYT-3, (b) XGBoost-HYT-CV, (c) RF-HYT, (d) ANNbN, (e) DANN-MPIH-HYT.

The ANNbN algorithm demonstrated varying performance in predicting the mechanical response of the pile-soil system. In Table 3, it is evident that ANNbN achieved a robust Pearson correlation of 98.38 % for *Fx Max* in the training set, which, however, significantly decreased to 86.12 % in the testing set (Fig. 9d). Notably, the prediction errors, specifically MAPE, exhibited a substantial increase from the training to the testing set (31.88 % to 62.15 %). Although a slightly improved MAPE was observed for both *Disp Max* (Fig. 10d) and *Disp Fx*2 (Fig. 11d) (27.66 % and 27.03 %, respectively, in Tables 4 and 5 for the testing set), similar trends of higher prediction errors for the test set compared to the train set derived.

For the case of the DANN-MPIH-HYT model, Table 3 shows a Pearson correlation of 92.45 % for *Fx Max* on the training set, with a similar value (92.38 %) when the predictive model is used for the testing set (Fig. 9e). However, prediction errors, were notably higher, reaching a 49.57 % MAPE for the training set and a 53.35 % for the testing set. Similarly, to ANNbN, an improved MAPE was achieved for both *Disp Max* (Fig. 10e) and *Disp Fx*2 (Fig. 11e) (25.09 % and 28.26 %, respectively, as seen in Tables 4 and 5 for the test set). Consequently, like ANNbN, DANN-MPIH-HYT demonstrated better performance in predicting displacements compared to horizontal failure forces.

Comparing the performance of the methods across the three target variables, the XGBoost-HYT-CV and RF-HYT-generated predictive models consistently demonstrate strong predictive capabilities, achieving the lowest MAPE in multiple instances. The POLYREG-HYT-3 method also was found to perform well, particularly when predicting *Fx Max*. However, it is essential to note that the performance of each method varies across the different target variables, highlighting the

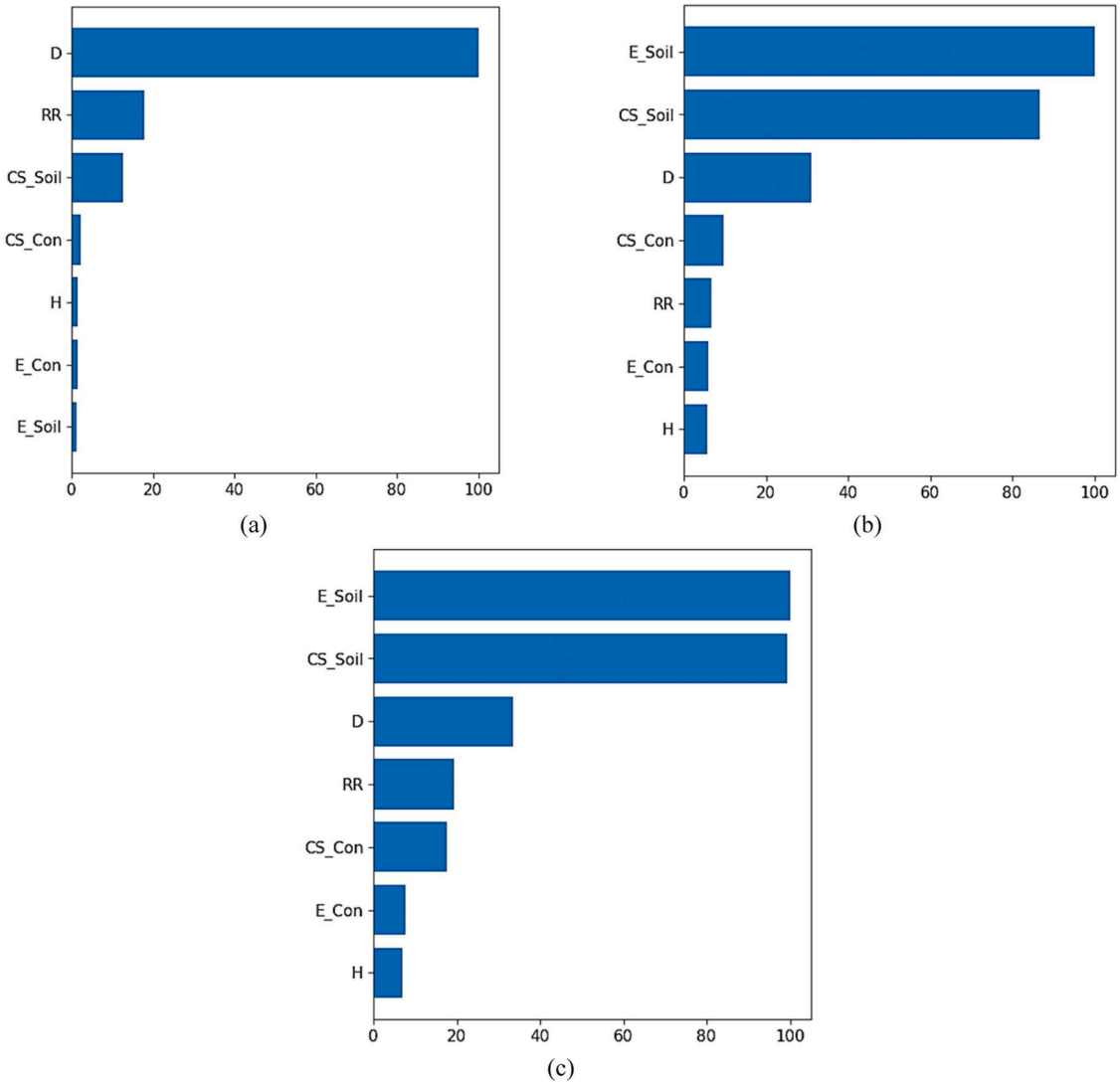

Fig. 12. XGBoost-HYT-CV sensitivity graph for input features with (a) *Fx Max*, (b) *Disp Max*, and (c) *Disp Fx*2.

importance of selecting an appropriate method based on the specific prediction task. The RF-HYT-generated predictive model was found to be the most accurate one in predicting *Fx Max* deriving the lowest error metrics when tested on the test dataset. Conversely, the XGBoost-HYT-CV model outperforms RF-HYT in terms of prediction accuracy for both *Disp Max* and *Disp Fx*2. This further emphasizes the superior robustness of the RF-HYT and XGBoost-HYT-CV predictive models compared to POLYREG-HYT-3 models across all three datasets.

Fig. 12 shows the sensitivity analysis performed by the XGBoost-HYT-CV algorithms during the training and testing of the predictive model of *Fx Max*, *Disp Max*, and *Disp Fx*2, respectively. According to the *Fx Max* sensitivity analysis graph (Fig. 12a), it is evident that the most important input feature is the pile diameter *D*, where the second most important is the reinforcement ratio *RR*. Therefore, even though these parameters were not investigated by Braun et al. [7], XGBoost-HYT-CV indicated features that were more sensitive to the system, specifically when predicting ultimate horizontal capacity *Fx Max*. Nevertheless, according to this sensitivity analysis the CS_{soil} was found to be the 3rd most important input feature, further validating the findings by Braun et al. [7].

Similar sensitivity graphs for the case of *Disp Max* and *Disp Fx*2 are provided in Fig. 12 (b) and (c), respectively. It is evident that both the E_{soil} and the CS_{soil} are the two most important parameters when it comes to computing the horizontal deformation of RC piles embedded in soil. This numerical finding further reinforces the findings reported by Braun et al. [7], where the parametric investigation of these parameters revealed that they were sensitive and strongly correlated to the ultimate capacity of the RC pile. It is also interesting to note here that the embedded pile length was found to be the least sensitive input feature that would affect the pile's horizontal deformation. This is attributed to the fact that all piles were embedded into soil for 6 or more meters, removing the case where the pile would have been under tension along its entire length. Therefore, the lower half of the piles would serve as a fixation during the horizontal deformation of the head of the pile.

6. Validation of predictive models

The validation of the proposed predictive models was performed with both the development of additional out-of-sample numerical data, as well as with the experimental results obtained from the WindAfrica project [13]. It is important to note at this point that the developed datasets did not include the numerical results obtained from the calibrated FE model presented by Braun et al. [7]. It is also of significant importance to note that the experimental results obtained from the WindAfrica project were also not included in the datasets that were used to train and test the proposed predictive models.

Out-of-sample model development foresaw the use of geometrical features and material properties that were not incorporated in any of the

Table 6
Geometrical (left) and material (right) parameters for out-of-sample models.

Geometrical Parameter	Value	Units	Material Parameter	Value	Units
Pile Diameter (D)	35, 55, 75	cm	Soil Young's modulus (E_{soil})	75, 125	MPa
Embedded Pile Depth (H)	7, 10	m	Soil compressive strength (CS_{soil})	52.5, 137.5	kPa
Reinforcement Ratio (ρ)	1, 2.5, 3	%	Concrete Young's modulus (E_{con})	30, 50	GPa
			Concrete compressive strength (CS_{con})	30, 50	MPa

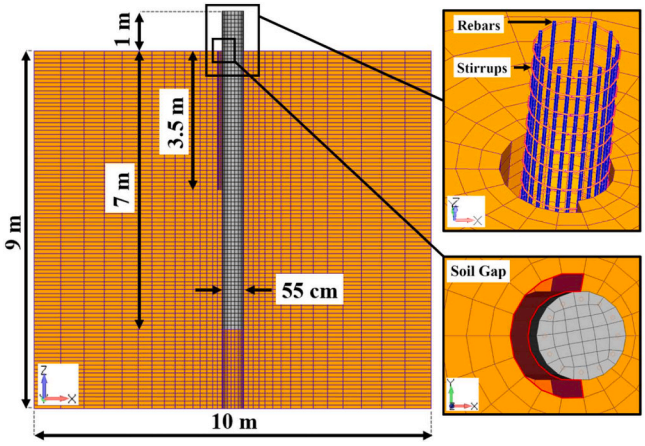

Fig. 13. Out-of-sample base model with a D of 55 cm, H of 7 m, and ρ of 2.5 %; reinforcement layout and interface of pile and soil detachment.

Table 7
Fx Max out-of-sample performance metrics.

ML Method	Pearson (%)	MAPE (%)	MAMPE (%)	MAE	RMSE
LR	92.66	41.43	24.48	66.607	81.539
POLYREG-HYT-3	97.00	**17.38**	**13.66**	37.149	47.645
XGBoost-HYT-CV	95.08	50.70	35.65	96.982	115.203
RF-HYT	97.13	28.13	21.29	57.929	66.856
ANNbN	92.71	62.22	41.87	113.922	129.810
DANN-MPIH-HYT	**97.32**	17.41	13.06	**35.519**	**43.325**

models that were used to develop the initial dataset. The aim was to ensure these new models no longer retained the same geometric configurations and material properties as used in the training and testing phases. Following the production of 18 base models through the use of the geometrical input features shown in Table 6, each model was then used to construct additional models based on all possible material parameter combinations. This procedure led to the development of 288 out-of-sample additional numerical models. Fig. 13 illustrates an example of one of the base models which has a specific combination in terms of geometry and material properties.

After the numerical models were analyzed, the same filter was used to develop the final validation dataset. This filter foresaw the inclusion of the models that derived displacement increments equal to or greater than 10 ($NR \geq 10$), whereas the final validation dataset foresaw a total of 156 out-of-sample datapoints. Notably, this restriction did not compromise the representation of the entire range of minimum, medium, and maximum geometrical and material property parameters according to Table 6.

Table 8
Disp Max out-of-sample performance metrics.

ML Method	Pearson (%)	MAPE (%)	MAMPE (%)	MAE	RMSE
LR	45.24	24.86	24.11	0.010	0.012
POLYREG-HYT-3	**53.49**	24.30	**22.00**	**0.009**	**0.011**
XGBoost-HYT-CV	49.90	26.85	22.49	0.009	0.011
RF-HYT	49.56	31.10	30.53	0.012	0.016
ANNbN	39.50	**23.86**	23.61	0.010	0.013
DANN-MPIH-HYT	0.4033	29.57	25.83	0.010	0.013

Table 9
Disp Fx2 out-of-sample performance metrics.

ML Method	Pearson (%)	MAPE (%)	MAMPE (%)	MAE	RMSE
LR	42.96	24.47	23.44	0.003	0.003
POLYREG-HYT-3	**54.61**	23.52	**21.10**	**0.002**	**0.003**
XGBoost-HYT-CV	44.11	25.25	21.53	0.002	0.003
RF-HYT	47.87	28.60	28.25	0.003	0.004
ANNbN	50.46	**22.56**	21.11	0.002	0.003
DANN-MPIH-HYT	46.63	24.88	22.39	0.003	0.003

Table 7 presents a comprehensive analysis of error metrics for the out-of-sample predictions when computing *Fx Max* by various ML models. Notably, POLYREG-HYT-3 and DANN-MPIH-HYT demonstrated superior performance, achieving strong Pearson correlations of 97 % and 97.32 %, low MAPEs of 17.38 % and 17.41 %, and low MAMPE values equal to 13.66 % and 13.06 %, respectively. Despite RF-HYT exhibiting a strong Pearson correlation of 97.13 %, it did not manage to derive optimum MAPE and MAMPE values compared to the POLYREG-HYT-3 and DANN-MPIH-HYT predictive models. Tables 8 and 9 present the error metrics for out-of-sample predictions of *Disp Max* and *Disp Fx*2, respectively. While all models showed weak Pearson correlations for both datasets, the POLYREG-HYT-3 predictive model was found to derive the strongest correlation of 53.49 % and 54.61 %, for the case of *Disp Max* and *Disp Fx*2, respectively. Interestingly, the ANNbN proposed predictive model achieved the lowest MAPE of 23.86 % and 22.56 % for both horizontal displacement datasets, demonstrating its capability to make accurate predictions on out-of-sample data. Fig. 14a showcases the predicted versus target plot for the DANN-MPIH-HYT model for *Fx Max*, displaying a strong linear correlation despite some outliers. Fig. 14 (b) and (c) illustrate the predicted versus target plot for the ANNbN model for *Disp Max* and *Disp Fx*2, respectively, indicating a weak linear correlation with scattered data points and outliers.

To further validate the proposed predictive models, their predictions were compared with experimental results from the WindAfrica project. Notably, and as stated above, the datasets used for training and testing the proposed predictive models excluded numerical results from the Braun et al. (2023) calibrated FE model and the WindAfrica experiment. By utilizing input parameters from the WindAfrica experiment, along with the back-calculated soil parameters obtained by Braun et al. [7], P-δ curves were generated through the use of the proposed ML-generated models presented in this research work. These curves were then compared to the experimental curve as shown in Fig. 15. The analysis revealed that POLYREG-HYT-3 and DANN-MPIH-HYT provided the best fit, demonstrating accuracy in predicting the lateral pile-soil system's mechanical response. Meanwhile, XGBoost-HYT-CV and RF-HYT offered acceptable representations, whereas LR and ANNbN did not accurately capture the system's behaviour, deviating from the experimentally obtained curve.

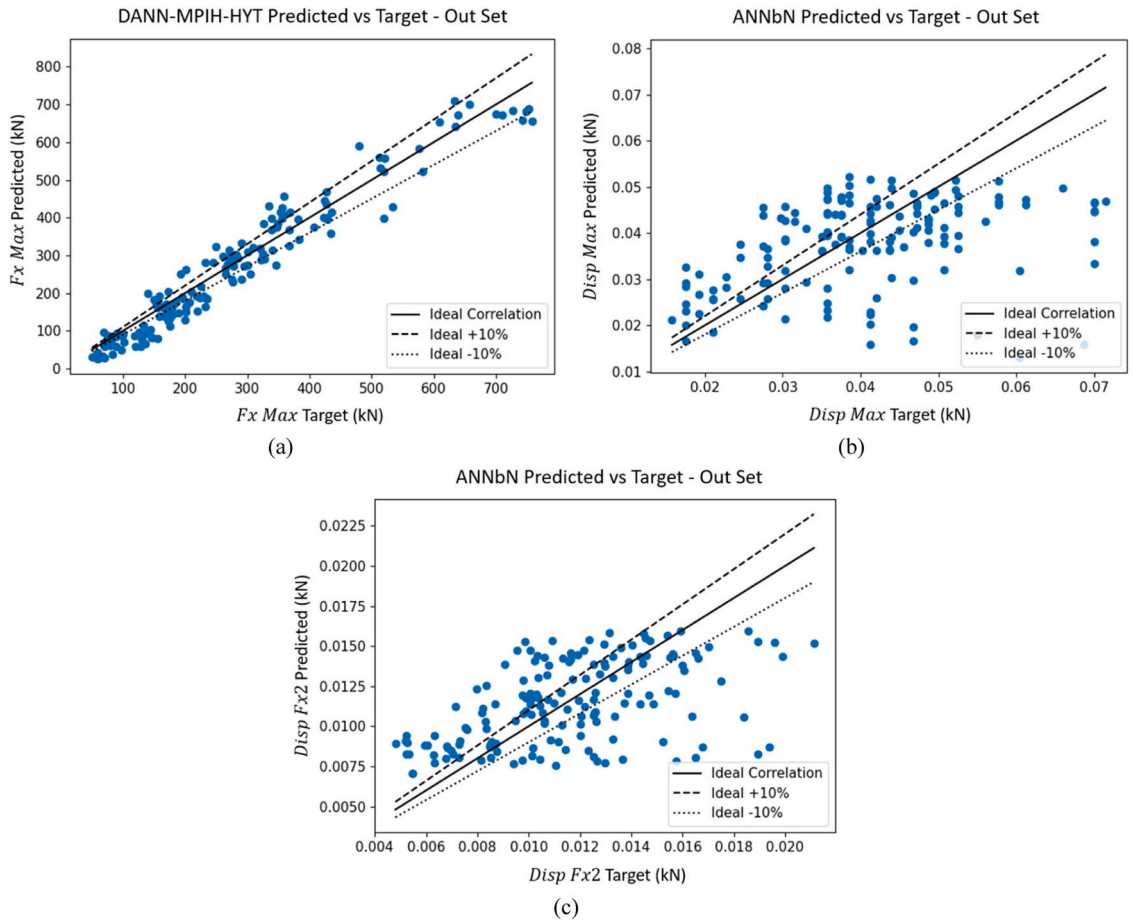

Fig. 14. Out-of-sample set target versus predicted plot. (a) DANN-MPIH-HYT for *Fx Max*, (b) ANNbN for *DispMax*, and (c) ANNbN for *Disp Fx*2.

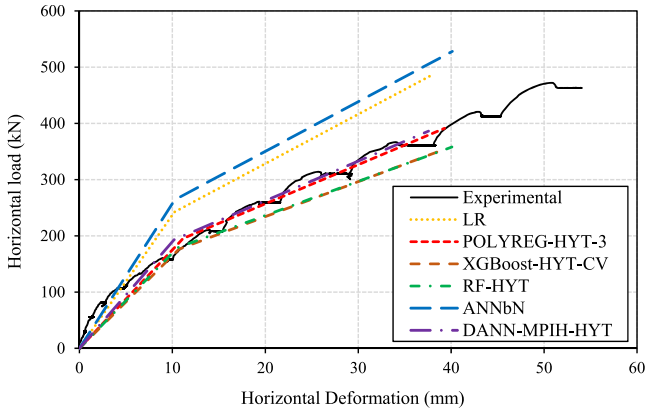

Fig. 15. Experimental and ML-generated model validation.

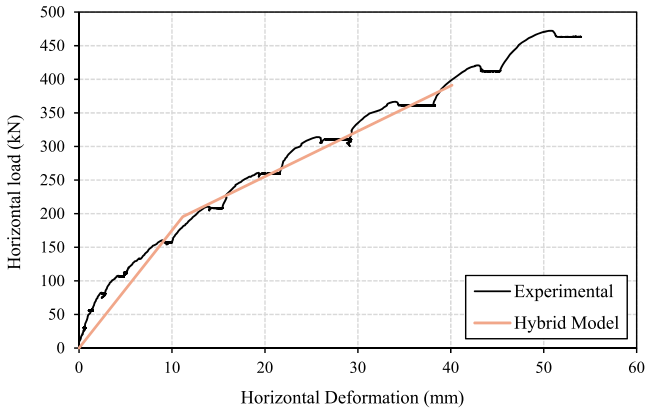

Fig. 16. Hybrid predictive model.

The POLYREG-HYT-3 predictive model was found to provide the most accurate P-δ curve among all proposed predictive models, accurately capturing the experimental data, whereas the prediction of the proposed model was in favor of safety when computing the ultimate capacity of the SSI system. To enhance accuracy, a hybrid predictive model (Fig. 16) was created by combining the best-performing ML-generated models, which foresaw the use of POLYREG-HYT-3 for predicting the *Fx Max* and *Disp Fx*2, and the ANNbN-generated predictive model for computing the *Disp Max*. The resulting optimal P-δ curve, which can be seen in Fig. 16, demonstrated an acceptable level of accuracy when compared to the experimental curve while being in favor of safety.

In Table 10, a summary of the test dataset performance metrics for each target variable for all adopted ML methods is presented. The best-performing error metric for each target variable has been bolded, indicating the ML method that performed the best for each performance metric, respectively. Notably, the lowest MAPE values for the test dataset are indicative of the best-performing ML method. For the *Fx Max* target variable, the RF-HYT method achieved the lowest MAPE of 13.02 %, followed closely by XGBoost-HYT-CV with 14.77 %. These methods also demonstrate low MAMPE, MAE, and RMSE values, indicating their effectiveness in predicting *Fx Max*. For both *Disp Max* and *Disp Fx*2, the XGBoost-HYT-CV was the best-performing ML method,

Table 10
Test set ML performance metrics for each Target Variable.

Target Variable	ML Method	Pearson (%)	MAPE (%)	MAMPE (%)	MAE	RMSE
Fx Max	LR	88.77	80.21	33.49	93.710	136.028
	POLYREG-HYT-3	98.48	20.43	11.91	33.313	50.899
	XGBoost-HYT-CV	**98.71**	14.77	**10.41**	**29.121**	**47.147**
	RF-HYT	98.52	**13.02**	10.56	29.548	52.206
	ANNbN	86.12	62.15	34.21	95.731	147.833
	DANN-MPIH-HYT	92.38	53.35	26.88	75.206	118.851
Disp Max	LR	66.10	26.48	23.86	0.010	0.013
	POLYREG-HYT-3	71.89	24.92	21.42	0.009	0.012
	XGBoost-HYT-CV	**72.65**	**24.20**	**20.59**	**0.009**	**0.011**
	RF-HYT	71.81	24.69	20.71	0.009	0.012
	ANNbN	66.83	27.66	23.74	0.010	0.012
	DANN-MPIH-HYT	72.16	25.09	21.90	0.009	0.012
Disp Max	LR	61.11	24.94	22.50	0.003	0.003
	POLYREG-HYT-3	70.14	22.07	19.01	0.002	0.003
	XGBoost-HYT-CV	**70.41**	**21.59**	**18.60**	**0.002**	**0.003**
	RF-HYT	69.72	21.76	18.65	0.002	0.003
	ANNbN	58.00	27.03	23.50	0.003	0.003
	DANN-MPIH-HYT	60.65	28.26	22.44	0.003	0.003

Table 11
Out-of-sample ML performance metrics for each Target Variable.

Target Variable (Out-of-sample)	ML Method	Pearson (%)	MAPE (%)	MAMPE (%)	MAE	RMSE
Fx Max	LR	92.66	41.43	24.48	66.607	81.539
	POLYREG-HYT-3	97.00	**17.38**	**13.66**	37.149	47.645
	XGBoost-HYT-CV	95.08	50.70	35.65	96.982	115.203
	RF-HYT	97.13	28.13	21.29	57.929	66.856
	ANNbN	92.71	62.22	41.87	113.922	129.810
	DANN-MPIH-HYT	**97.32**	17.41	13.06	**35.519**	**43.325**
Disp Max	LR	45.24	24.86	24.11	0.010	0.012
	POLYREG-HYT-3	**53.49**	24.30	**22.00**	**0.009**	**0.011**
	XGBoost-HYT-CV	49.90	26.85	22.49	0.009	0.011
	RF-HYT	49.56	31.10	30.53	0.012	0.016
	ANNbN	39.50	**23.86**	23.61	0.010	0.013
	DANN-MPIH-HYT	0.4033	29.57	25.83	0.010	0.013
Disp Fx2	LR	42.96	24.47	23.44	0.003	0.003
	POLYREG-HYT-3	**54.61**	23.52	**21.10**	**0.002**	**0.003**
	XGBoost-HYT-CV	44.11	25.25	21.53	0.002	0.003
	RF-HYT	47.87	28.60	28.25	0.003	0.004
	ANNbN	50.46	**22.56**	21.11	0.002	0.003
	DANN-MPIH-HYT	46.63	24.88	22.39	0.003	0.003

producing the lowest MAPE values of 24.20 % and 21.59 %, respectively. For both displacement target variables, XGBoost-HYT-CV also showed the highest Pearson correlation and the lowest MAMPE, MAE, and RMSE values, enhancing the proposed predictive models' effectiveness in predicting displacements.

Table 11 presents a summary of the out-of-sample performance metrics for each ML method for each target variable that was investigated for the needs of this research work. As seen within the table, the best-performing error metric for each target variable has been bolded, indicating the ML method that performed the best for each performance metric. For *Fx Max*, the POLYREG-HYT-3 ML algorithm achieved the lowest MAPE equal to 17.38 %. Furthermore, for both *Disp Max* and *Disp Fx*2, the ANNbN ML algorithm derived the lowest MAPE values of 23.86 % and 22.56 %, respectively.

7. Conclusions and recommendations

This study aimed to create multiple numerical models using various geometrical configurations and material properties, generating a large dataset to train and test ML algorithms. Once this was achieved, predictive models were created to predict the horizontal failure force and displacement of RC piles for a given set of input features. The three developed datasets were based on experimentally validated 3D detailed models.

The modelling process involved a VBA code for automating the replication of base models and adjusting material parameters systematically. This resulted in 6561 numerical models, constituting the largest pile-soil interaction dataset in the international literature. After simulating each numerical model through Reconan FEA [34] and generating three datasets, ML algorithms were then used to train predictive models for computing the horizontal failure force and displacement of the piles.

Results showed that RF-HYT outperformed all predictive models during training, achieving low MAPE values. For the case of the test set, RF-HYT excelled in predicting horizontal forces, while XGBoost-HYT-CV outperformed all the methods when dealing with the prediction of horizontal displacements. Sensitivity analysis revealed that pile diameter influenced force predictions, while soil properties influenced the prediction of horizontal displacements. The predictive models were further validated using an out-of-sample dataset, with POLYREG-HYT-3 emerging as the most accurate for force predictions, while DANN-MPIH-HYT performed optimally for displacements.

To further validate the predictive models, a RC pile embedded in unsaturated clay that was experimentally tested was used. The predictive models that managed to capture the P-δ curve most accurately were the POLYREG-HYT-3 and DANN-MPIH-HYT reproducing the nonlinear mechanical response with an acceptable accuracy. Thereafter, a hybrid predictive model was proposed that combines the optimal features of the different proposed predictive models that were developed for the needs of this research work. According to the proposed hybrid predictive model, POLYREG-HYT-3 is used for force capacity computations and the

prediction of the horizontal displacement for a horizontal force that is half of the ultimate capacity, where ANNbN is used to predict the horizontal displacement at the point of failure. Finally, it is recommended that the proposed predictive models be used for values that are within the minimum and maximum values used to train and test the proposed models.

According to the parametric investigation and the predictive model analysis, future research work is required to further extend the existing datasets that will allow the development of predictive models that will be applicable to a larger spectrum of geometries. Additionally, the investigation of multilayered soil profiles is required to be performed, where piles will be assumed to be found within a rock layer. For the needs of further validating the proposed predictive models, it is of significant importance to perform additional experiments with RC piles that have different diameters and are found within soil domains of various mechanical properties.

CRediT authorship contribution statement

Kevin Theodor Braun: Writing – review & editing, Writing – original draft, Visualization, Validation, Supervision, Software, Resources, Project administration, Methodology, Investigation, Funding acquisition, Formal analysis, Data curation, Conceptualization. **George Markou:** Writing – review & editing, Supervision, Software,Resources. **Schalk Jacobsz:** Supervision. **Duan Calitz:** Resources.

Declaration of Competing Interest

The authors declare that they have no known competing financial interests or personal relationships that could have appeared to influence the work reported in this paper.

Appendix A. Supporting information

Supplementary data associated with this article can be found in the online version at doi:10.1016/j.istruc.2024.106532.

References

[1] Alhamaydeh M, Markou G, Bakas N, Papadrakakis M. AI-based shear capacity of FRP-reinforced concrete deep beams without stirrups. Eng Struct 2022;264:114441.
[2] Al-Hussaini T. Soil-foundation-structure interaction analysis. Encyclopedia of LIfe Support Systems (EOLSS). Oxford, UK: Eolss Publishers; 2019.
[3] Atkinson JH, Bransby P. The mechanics of soils: an introduction to critical state soil mechanics. New York, NY United States: McGraw-Hill; 1978.
[4] Bakas N, Langousis A, Nicolaou M, Chatzichristofis S. Gradient free stochastic training of ANNs, with local approximation in partitions. Stoch Environ Res Risk Assess 2023:1–15.
[5] Basu D, Salgado R, Prezzi M. Analysis of laterally loaded piles in multilayered soil deposits. Jt Transp Res Program 2008:330.
[6] Bengio Y, Goodfellow I, Courville A. Deep learning. Cambridge, MA, USA: MIT Press; 2017.
[7] Braun K, Bakas N, Markou G, Jacobsz S. Advanced numerical modelling of the nonlinear mechanical behaviour of a laterally loaded pile embedded in stiff unsaturated clay. J South Afr Inst Civ Eng 2023;65(2):28–38.
[8] Breiman L. Random forests. Mach Learn 2001;45:5–32.
[9] Chen M, Challita U, Saad W, Yin C, Debbah M. Artificial neural networks-based machine learning for wireless networks: a tutorial. IEEE Commun Surv Tutor 2019;21(4):3039–71.
[10] Chore H, Ingle R, Sawant V. Non-linear analysis of pile groups subjected to lateral loads using 'p-y'curve. Interact Multiscale Mech 2012;5(1):57–73.
[11] Felippa CA. Introduction to finite element methods. Univ Colo 2004;885.
[12] Filippou FC, Popov EP, Bertero VV. National Science Foundation. ReportUCB/EERC-83/19. Effects of bond deterioration on hysteretic behavior of reinforced concrete joints. California: Berkeley; 1983.
[13] Gaspar T, Osman A, Aubeny C, Coombs W. Performance-based design of pile foundations for wind turbines in African unsaturated expansive soils. In: Proceedings of twentieth international conference on soil mechanics and geotechnical engineering, Sydney 2022.
[14] Gravett DZ, Markou G. State-of-the-art investigation of wind turbine structures founded on soft clay by considering the soil-foundation-structure interaction phenomenon–Optimization of battered RC piles. Eng Struct 2021;235:112013.
[15] Gravett DZ, Mourlas C, Taljaard V-L, Bakas N, Markou G, Papadrakakis M. New fundamental period formulae for soil-reinforced concrete structures interaction using machine learning algorithms and ANNs. Soil Dyn Earthq Eng 2021;144:106656.
[16] Ismail MIS, Okamoto Y, Okada A. Neural network modeling for prediction of weld bead geometry in laser microwelding, 6th August 2023 2013. https://www.hindawi.com/journals/aot/2013/415837/.
[17] Jardine R, Potts D, Fourie A, Burland J. Studies of the influence of non-linear stress–strain characteristics in soil–structure interaction. Geotechnique 1986;36(3):377–96.
[18] Karthigeyan S, Ramakrishna V, Rajagopal K. Influence of vertical load on the lateral response of piles in sand. Comput Geotech 2006;33(2):121–31.
[19] Kausel E. Early history of soil–structure interaction. Soil Dyn Earthq Eng 2010;30(9):822–32.
[20] Kavitha P, Beena K, Narayanan K. A review on soil–structure interaction analysis of laterally loaded piles. Proc Innov Infrastruct Solut 2016;1:1–15.
[21] Kotsovos MD, Pavlovic MN. Structural concrete: finite-element analysis for limit-state design. Thomas Telford; 1995.
[22] Markou GA. Detailed three-dimensional nonlinear hybrid simulation for the analysis of large-scale reinforced concrete structures [PhD thesis]. National Technical University of Athenst 2011.
[23] Markou G, Bakas NP. Prediction of the shear capacity of reinforced concrete slender beams without stirrups by applying artificial intelligence algorithms in a big database of beams generated by 3D nonlinear finite element analysis. Comput Concr 2021;28(6):433–47.
[24] Markou G, Papadrakakis M. Computationally efficient 3D finite element modeling of RC structures. Comput Concr 2013;12(4):443–98.
[25] Markou G, Roeloffze W. Finite element modelling of plain and reinforced concrete specimens with the Kotsovos and Pavlovic material model, smeared crack approach and fine meshes. Int J Damage Mech 2021. 1056789520986601.
[26] Markou G, Bakas N, Chatzichristofis S, Papadrakakis M. A general framework of high-performance machine learning algorithms: application in structural mechanics. Comput Mech 2024;73:705–29.
[27] Menegotto M. Method of analysis for cyclically loaded RC plane frames including changes in geometry and non-elastic behavior of elements under combined normal force and bending. In: Proc. of the IABSE symposium on resistance and ultimate deformability of structures acted on by well defined repeated loads 1973:15–22.
[28] Mitchell R. GPU Accelerated XGBoost 2016. <https://xgboost.ai/2016/12/14/GPU-accelerated-xgboost.html>.
[29] Mourlas C, Markou G, Papadrakakis M. Accurate and computationally efficient nonlinear static and dynamic analysis of reinforced concrete structures considering damage factors. Eng Struct 2019;178:258–85.
[30] Moussa A, Christou P. The evolution of analysis methods for laterally loaded piles through time. In: Advances in analysis and design of deep foundations: proceedings of the first GeoMEast International Congress and Exhibition, Egypt 2017 on sustainable civil infrastructures 1. Springer; 2018. p. 65–94.
[31] Park J. Dynamic response of a single pile and group piles in sands by three dimensional analysis [Ph.D. thesis]. Seoul, Korea: Yonsei University; 2018.
[32] Pedregosa F, Varoquaux G, Gramfort A, Michel V, Thirion B, Grisel O, et al. Scikit-learn: machine learning in Python. J Mach Learn Res 2011;12:2825–30.
[33] Rademan, D. , Markou, G. 2023. Investigating the soil stress levels for different pile geometries under different loading configurations. In: Proceedings of COMPDYN (Papadrakakis, M., and Fragiadakis, M. (eds)).
[34] Reconan Fea V2.00, User's Manual 2020. Available from: https://www.researchgate.net/publication/342361609_ReConAn_v200_Finite_Element_Analysis_Software_User's_Manual.
[35] Reese LC, Isenhower WM, Wang S-T. Analysis and design of shallow and deep foundations. John Wiley & Sons; 2005.
[36] Smith I. Smith's elements of soil mechanics. John Wiley & Sons; 2021.
[37] Thai H-T. Machine learning for structural engineering: a state-of-the-art review. Structures 2022;38:448–91.
[38] Ti KS, Huat BB, Noorzaei J, Jaafar MS, Sew GS. A review of basic soil constitutive models for geotechnical application. Electron J Geotech Eng 2009;14:1–18.
[39] van Der Westhuizen AM, Bakas, N AM, G MARKOU. Developing an artificial neural network model that predicts the fundamental period of steel structures using a large dataset. In: Proceedings of COMPDYN. Greece: Athens; 2023.
[40] van Der Westhuizen AM, Markou G, Bakas N. Development of a new fundamental period formula for steel structures considering the soil-structure interaction with the use of machine learning algorithms. ICAART 2022;(3):952–7.
[41] Weisstein EW. Least Squares Fitting 2002. Available from: <https://mathworld.wolfram.com/LeastSquaresFitting.html>. [Accessed 20 June 2023].
[42] Willam KJ. Constitutive model for the triaxial behavior of concrete. IABSE Semin Concr Struct Subj Triaxial Stress 1974:1–30.

Update

Structures

Volume 65, Issue , July 2024, Page

DOI: https://doi.org/10.1016/j.istruc.2024.106757

Structures 65 (2024) 106757

Contents lists available at ScienceDirect

Structures

journal homepage: www.elsevier.com/locate/structures

Corrigendum

Corrigendum to "Developing predictive models for the load-displacement response of laterally loaded reinforced concrete piles in stiff unsaturated clay using machine learning algorithms" [Structures 64 (2024) 1–15/106532]

K.T. Braun [a,*], G. Markou [a,b], S.W. Jacobsz [a], D. Calitz [c]

[a] Civil Engineering Department Hatfield Campus, University of Pretoria, South Africa
[b] Department of Civil Engineering, Neapolis University Pafos, 2 Danais Avenue, Pafos 8042, Cyprus
[c] SRK Consulting, 265 Oxford Rd, Illovo, Johannesburg, South Africa

The authors regret "In Table 8 and Table 11 the Pearson (%) value for DANN-MPIH-HYT for Disp Max, needs to be 40.33 and not 0.4033".

The authors would like to apologise for any inconvenience caused.

DOI of original article: https://doi.org/10.1016/j.istruc.2024.106532.
* Corresponding author.
E-mail address: u17031215@tuks.co.za (K.T. Braun).

https://doi.org/10.1016/j.istruc.2024.106757

Available online 21 June 2024